Supplementary Information

Triangulo-{Er^{III}_3} complex showing field supported slow magnetic relaxation

Mamo Gebrezgiabher[a,b], Sören Schlittenhardt[c], Cyril Rajnák[b], Juraj Kuchár[d], Assefa Sergawie[a], Juraj Černák[d], Mario Ruben[c,f,g], Madhu Thomas[a,*] and Roman Boča[b,*]

[a]Department of Industrial Chemistry, College of Applied Sciences, Nanotechnology Excellence Center, Addis Ababa Science and Technology University, Addis Ababa P.O. Box 16417, Ethiopia.

[b]Department of Chemistry, Faculty of Natural Sciences, University of SS Cyril and Methodius 91701 Trnava, Slovakia.

[c]Institute of Nanotechnology, Karlsruhe Institute of Technology, Hermann-von-Helmholtz-Platz 1, 76344 Eggenstein-Leopoldshafen, Germany.

[d]Department of Inorganic Chemistry, Institute of Chemistry, P. J. Šafárik University in Košice, 041 80 Košice, Slovakia.

[e]Institute of Quantum Materials and Technologies (IQMT), Karlsruhe Institute of Technology, Hermann-von-Helmholtz-Platz 1, 76344 Eggenstein-Leopoldshafen, Germany.

[f]Centre Européen de Science Quantique (CESQ); Institut de Science et d'Ingénierie Supramoléculaires (ISIS, UMR 7006), CNRS-Université de Strasbourg, 8 allée Gaspard Monge BP 70028 67083 Strasbourg Cedex, France.

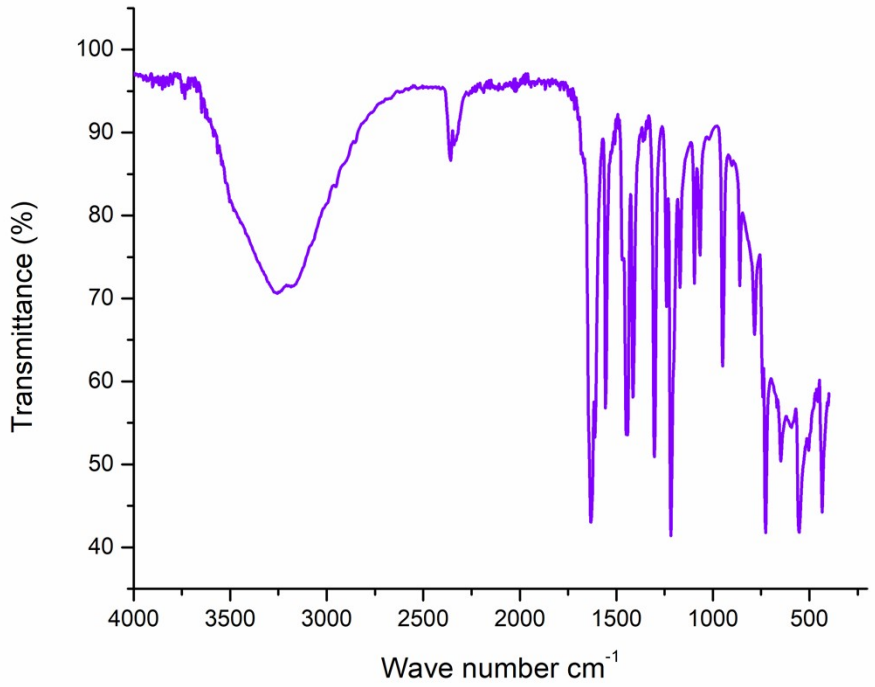

Fig. S1. IR spectrum of complex **1**.

Table S1. Results of the Continuous Shape Measures calculations

---

S H A P E v2.1: Continuous Shape Measures calculation (c) 2013 Electronic Structure Group, Universitat de Barcelona Contact: llunell@ub.edu

---

OP-8	1	D_8h	Octagon
HPY-8	2	C_7v	Heptagonal pyramid
HBPY-8	3	D_6h	Hexagonal bipyramid
CU-8	4	Oh	Cube
SAPR-8	5	D_4d	Square antiprism
TDD-8	6	D_2d	Triangular dodecahedron
JGBF-8	7	D_2d	Johnson gyrobifastigium J26
JETBPY-8	8	D_3h	Johnson elongated triangular bipyramid J14
JBTPR-8	9	C_2v	Biaugmented trigonal prism J50
BTPR-8	10	C_2v	Biaugmented trigonal prism
JSD-8	11	D_2d	Snub diphenoid J84
TT-8	12	Td	Triakis tetrahedron
ETBPY-8	13	D_3h	Elongated trigonal bipyramid

a) ErD_8 in **1**

Structure **1**												
[ML_8]	OP-8	HPY-8	HBPY-8	CU-8	SAPR-8	TDD-8	JGBF-8	JETBPY-8	JBTPR-8	BTPR-8	JSD-8	TT-8	ETBPY-8
Er1,	31.934,	22.220,	16.116,	10.187,	2.852,	**0.909**,	14.964,	29.632,	3.389,	2.877,	3.518,	10.830,	24.556
Er2,	31.824,	22.070,	15.266,	9.505,	2.908,	**0.540**,	14.735,	29.004,	2.930,	2.532,	2.878,	10.365,	24.265
Er3,	30.623,	22.103,	15.261,	11.111,	1.871,	**0.921**,	13.624,	28.313,	2.634,	1.989,	2.808,	11.830,	24.295

The polyhedra are close to **triangular dodecahedrons**

b) ErD_8 in $[Er_3Cl_3(o\text{-}van\text{Br})_3(OH)_2(CH_3OH)_3]Cl\cdot 3CH_3OH$[1]

Structure [ML_8]	OP-8	HPY-8	HBPY-8	CU-8	SAPR-8	TDD-8	JGBF-8	JETBPY-8	JBTPR-8	BTPR-8	JSD-8	TT-8	ETBPY-8
Er1p*,	30.146,	22.412,	16.318,	10.369,	2.082,	0.629,	14.266,	29.362,	2.278,	1.695,	2.921,	11.135,	23.937
Er2p*,	30.320,	21.582,	16.475,	10.406,	2.183,	1.077,	15.133,	29.372,	2.683,	2.042,	3.733,	11.036,	23.245
Er3p*,	31.941,	22.932,	16.363,	10.690,	2.954,	0.986,	15.242,	29.401,	3.593,	2.496,	4.048,	11.049,	23.816

The polyhedra are close to **triangular dodecahedrons**

Table S2 Possible hydrogen bonds in **1** [Å, °].

D-H···A	D-H	H···A	D···A	DHA
O10–H10O···Cl2^{i}	0.84	2.47	3.268(3)	161
O11–H11O···Cl3	0.84	2.48	3.274(3)	158
O21–H21A···Cl2^{ii}	0.83	2.25	3.041(4)	159
O21–H21B···Cl2^{i}	0.84	2.38	3.212(4)	170
O22–H22A···Cl3	0.84	2.40	3.175(4)	154
O22–-H22B···O35A	0.84	1.84	2.669(8)	168
O23–H23A···Cl3^{iii}	0.84	2.26	3.100(4)	176
O23–H23B···Cl3	0.84	2.33	3.157(4)	166

O24–H24A···Cl1^{iv}	0.84	2.32	3.161(3)	177
O24–H24B···O34	0.84	1.88	2.724(7)	175
O25–H25A···Cl2^{i}	0.84	2.305	3.126(3)	165
O25–H25B···Cl4B^{i}	0.84	2.34	3.173(5)	171
O25–H25B···O31^{i}	0.84	1.78	2.609(9)	169

Symmetry codes: i: 1-x, -1/2+y, 1/2-z; ii: -1/2+x, 1-y, z; iii: 1-x, 1-y, 1-z; iv: 1/2+x, 1-y, z.

Table S3. Crystal data and structure refinement for **1**.

Empirical formula	$C_{24}H_{33}O_{25.47}Cl_4Er_3$
Formula weight	1372.613
Temperature/K	95.15
Crystal system	monoclinic
Space group	I2/a
a/Å	17.1520(3)
b/Å	17.8706(4)
c/Å	30.2439(6)
α/°	90
β/°	97.7617(18)
γ/°	90
Volume/Å^3	9185.3(3)
Z	8
ρ_{calc}g/cm^3	1.985
μ/mm^{-1}	5.743
F(000)	5230.3
Crystal size/mm^3	yellow block 0.204 × 0.125 × 0.118
Radiation / Å	Mo Kα (λ = 0.71073)
2*Θ* range for data collection/°	4.08 – 53.00
Index ranges	$-23 \leq h \leq 22$ $-23 \leq k \leq 23$ $-25 \leq l \leq 40$

Reflections collected	25470
Independent reflections	9623 [R_{int} = 0.0241, R_{sigma} = 0.0344]
Data/restraints/parameters	9623/17/613
Goodness-of-fit on F^2	1.067
Final R indexes [I ≥>=2σ (I)]	R_1 = 0.0303, wR_2 = 0.0674
Final R indexes [all data]	R_1 = 0.0389, wR_2 = 0.0710
Largest diff. peak/hole / e.Å^{-3}	1.84/-1.53

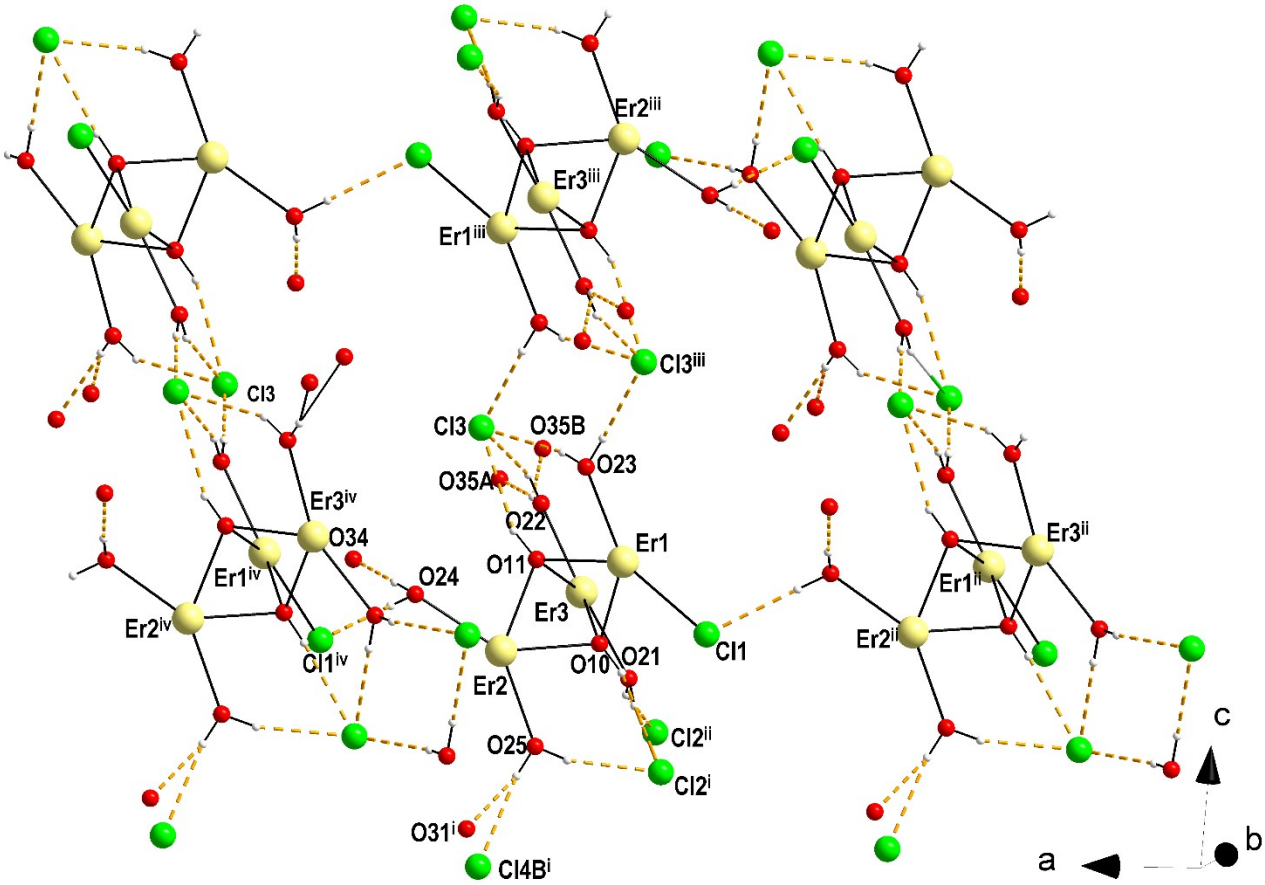

Fig. S2. View on hydrogen bonding system in **1** formed by O-H···O and O-H···Cl hydrogen bonds. Symmetry codes: i: 1-x, y-0.5, 0.5-z; ii: x-0.5, 1-y, z; iii: 1-x, 1-y, 1-z; iv: 0.5+x, 1-y, z.

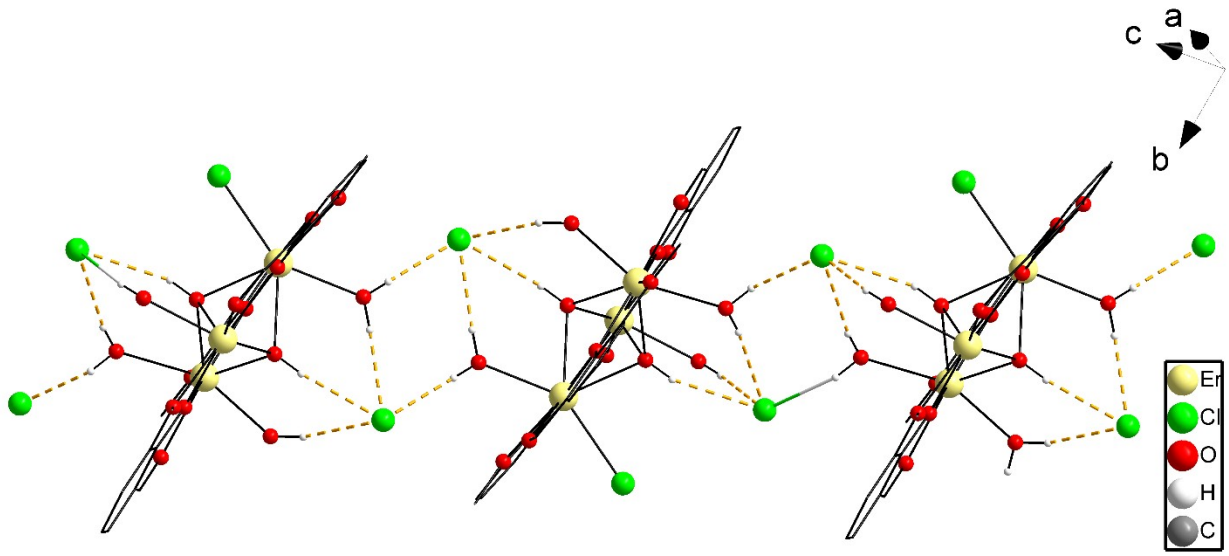

Fig.S3. View on the chain-like arrangement of trinuclear $\{Er_3\}$ entities linked by hydrogen bonds of the O-H···Cl type. Only hydrogen atoms involved in the propagation of chains are shown.

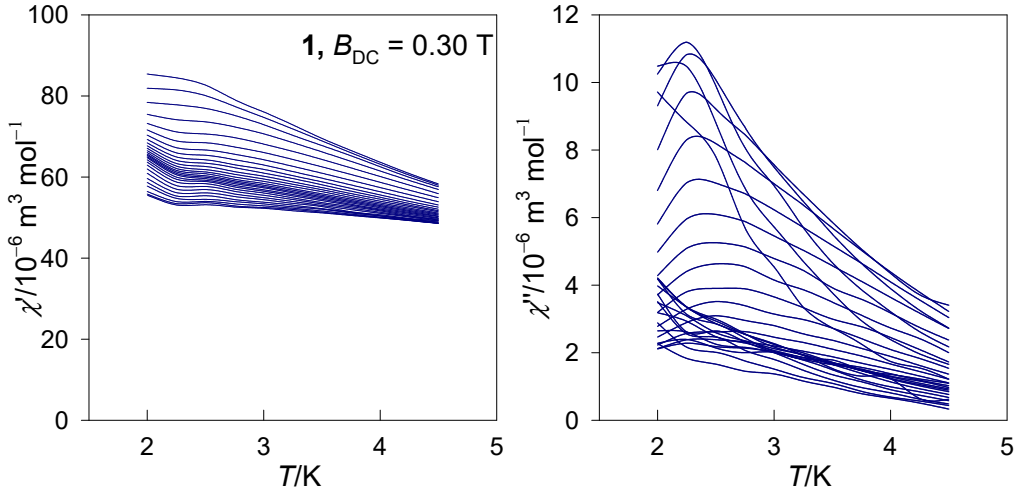

Fig. S4. Temperature dependence of the AC susceptibility for **1** at B_{DC} = 0.3 T depending upon the frequency of the AC field.

The Debye equation for AC susceptibility can be extended to the *two-set Debye model*

$$\chi(\omega) = \chi_S + \frac{\chi_{T1} - \chi_S}{1 + (\mathrm{i}\omega\tau_1)^{1-\alpha_1}} + \frac{\chi_{T2} - \chi_{T1}}{1 + (\mathrm{i}\omega\tau_2)^{1-\alpha_2}}$$

which splits into the in-phase component

$$\chi'(\omega) = \chi_S + (\chi_{T1} - \chi_S)\frac{1 + (\omega\tau_1)^{1-\alpha_1}\sin(\pi\alpha_1/2)}{1 + 2(\omega\tau_1)^{1-\alpha_1}\sin(\pi\alpha_1/2) + (\omega\tau_1)^{2-2\alpha_1}}$$
$$+(\chi_{T2} - \chi_{T1})\frac{1 + (\omega\tau_2)^{1-\alpha_2}\sin(\pi\alpha_2/2)}{1 + 2(\omega\tau_2)^{1-\alpha_2}\sin(\pi\alpha_2/2) + (\omega\tau_2)^{2-2\alpha_2}}$$

and the out-of-phase component

$$\chi''(\omega) = (\chi_{T1} - \chi_S)\frac{(\omega\tau_1)^{1-\alpha_1}\cos(\pi\alpha_1/2)}{1 + 2(\omega\tau_1)^{1-\alpha_1}\sin(\pi\alpha_1/2) + (\omega\tau_1)^{2-2\alpha_1}}$$
$$+(\chi_{T2} - \chi_{T1})\frac{(\omega\tau_2)^{1-\alpha_2}\cos(\pi\alpha_2/2)}{1 + 2(\omega\tau_2)^{1-\alpha_2}\sin(\pi\alpha_2/2) + (\omega\tau_2)^{2-2\alpha_2}}$$

with the constraint for the isothermal and adiabatic susceptibilities $\chi_S < \chi_{T1} < \chi_{T2}$ in order to get positive contributions from each primitive component.

Table S4. Fitted AC susceptibility data at T = 2.0 K [a]

B/T	χ_S	χ_{LF}	α_{LF}	τ_{LF}/s	χ_{HF}	α_{HF}	τ_{HF}/μs	x_{LF}
0.1	112	116	.06	**0.195**	125	.39	**239**	0.30
0.2	79	98	.31	**0.618**	111	.23	**413**	0.61
0.3	55	87	.38	**1.46**	99	.16	**504**	0.74
0.4	39	64	.37	**1.09**	74	.15	**542**	0.74
0.5	29	56	.42	**2.00**	63	.10	**560**	.80

[a] AC susceptibility components in unit of 10^{-6} m^3 mol^{-1} [SI].

Table S5. Fitted AC susceptibility data at B_{DC} = 0.3 T

T/K	χ_S	χ_{LF}	α_{LF}	τ_{LF}/s	χ_{HF}	α_{HF}	τ_{HF}/ms [a]	x_{LF}
2.00	54	86	.29	**1.23**	98	.24	**0.62**	0.73
2.25	51	80	.19	**0.73**	92	.38	**0.86**	0.71
2.50	51	79	.24	**0.63**	89	.36	**0.67**	0.74
2.75	50	73	.20	**0.47**	83	.44	**0.80**	0.69
3.00	50	69	.17	**0.42**	78	.50	**1.00**	0.66
3.25	50	66	.15	**0.37**	75	.50	**1.26**	0.65
3.50	49	61	.09	**0.35**	71	.60	**2.86**	0.54
3.75	49	59	.07	**0.32**	67	.60	**4.11**	0.55
4.00	49	57	.05	**0.30**	64	.58	**4.51**	0.52
4.25	48	55	.03	**0.29**	62	.59	**8.49**	0.50
4.50	48	53	.01	**0.29**	59	.55	**8.53**	0.52

[a] Note, the high-frequency relaxation time on heating <u>is not decreasing</u> (as usual) but increasing! This is a "reciprocating thermal behaviour".

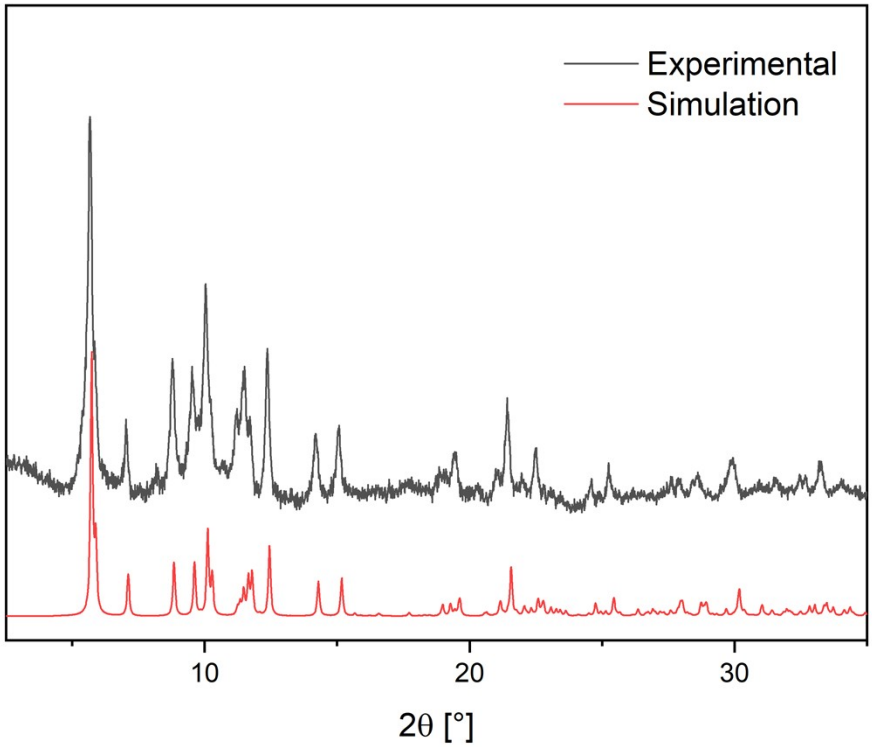

Fig. S5 X-ray powder diffraction patterns of 1 (simulated and experimental).

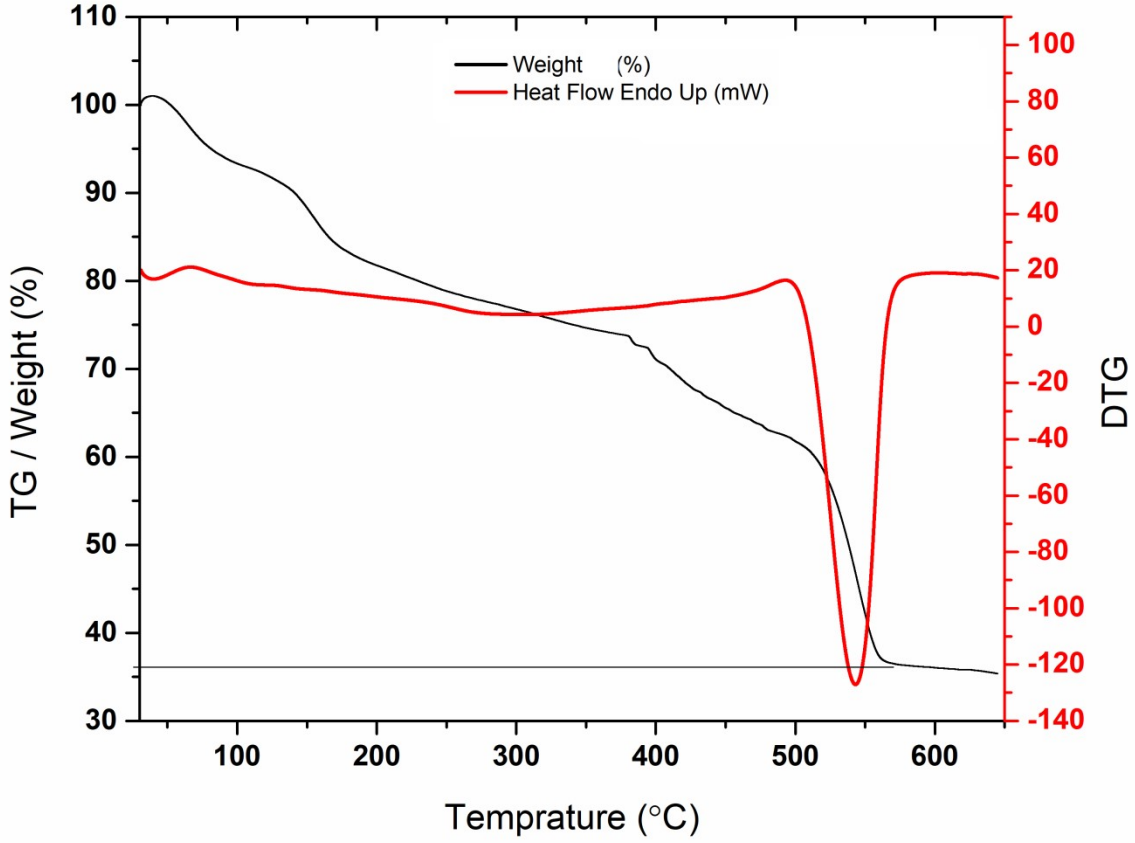

Fig.S6. Thermogravometric analysis curve for complex **1**.

Reference

1 X. Yang, R. A. Jones and M. J. Wiester, *Dalt. Trans.*, 2004, **3**, 1787–1788.